

On the direct assimilation of along-track sea-surface height observations into a free-surface ocean model using a weak constraints four-dimensional variational (4D-Var) method

Hans Ngodock,^{a*} Matthew Carrier,^a Innocent Souopgui,^b Scott Smith,^a Paul Martin,^a Philip Muscarella^a and Gregg Jacobs^a

^aThe Naval Research Lab, Stennis Space Center, MS, USA

^bDepartment of Marine Sciences, University of Southern Mississippi, Stennis Space Center, MS, USA

*Correspondence to: H. Ngodock, 1009 Balch Blvd, Stennis Space Center, MS 39529, USA. E-mail: hans.ngodock@nrlssc.navy.mil

The representer method is adopted for solving a weak constraints 4D-Var problem for the assimilation of ocean observations including along-track sea-surface height (SSH), using a free-surface ocean model. Direct 4D-Var assimilation of SSH observations along the satellite tracks requires that the adjoint model be integrated with Dirac impulses on the right-hand side (rhs) of the adjoint equations for the surface elevation equation. The solution of this adjoint model will inevitably include surface gravity waves, and it constitutes the forcing for the tangent linear model (TLM) according to the representer method. This yields an analysis that is contaminated by gravity waves. A method for avoiding the generation of the surface gravity waves in the analysis is proposed in this study; it consists of removing the adjoint of the free surface from the rhs of the free-surface mode in the TLM. The information from the SSH observations will still propagate to all other variables via the adjoint of the balance relationship between the barotropic and baroclinic modes, resulting in the correction to the surface elevation. Two assimilation experiments are carried out in the Gulf of Mexico: one with adjoint forcing included on the rhs of the TLM free-surface equation, and the other without. Both analyses are evaluated against the assimilated SSH observations, SSH maps from AVISO and independent surface drifters, showing that the analysis that did not include adjoint forcing in the free surface is more accurate. This study shows that when a weak constraints 4D-Var approach is considered for the assimilation of along-track SSH observations using a free-surface model, with the aim of correcting the mesoscale circulation, an independent model error should not be assigned to the free surface.

Key Words: data assimilation; along-track SSH; weak constraints 4D-Var; representer method

Received 2 February 2015; Revised 10 November 2015; Accepted 25 November 2015; Published online in Wiley Online Library 3 February 2016

1. Introduction

Prior studies observed planetary-scale waves expressed in the ocean surface (Luther, 1980) as waves such as (i) barotropic Kelvin waves due to wind and tidal forcing (LeBlonde and Lawrence, 1978; Knox and Halpern, 1982; Johnson and McPhaden, 1993), (ii) baroclinic Kelvin waves due to episodic forcing such as those observed during El Niño along the equatorial Pacific and American continental west coasts (Enfield and Allen, 1983; Spillane *et al.*, 1987), or (iii) baroclinic Rossby waves due to the reflection of Kelvin waves (Moore, 1968; Moore and McCreary, 1990; Perigaud and Delecluse, 1992; Jacobs *et al.*, 1994). Tsunamis are well known barotropic waves associated with underwater seismic disturbances (Nosov, 2014). Other oceanic barotropic waves are associated with atmospheric gravity waves, pressure

jumps, frontal passages, squalls, etc., which normally generate barotropic ocean waves in the open ocean and amplify them near the coast (Monserrat *et al.*, 2006).

Prior studies also observed geostrophically balanced mesoscale eddies across the globe that affect the ocean-surface height through steric variations throughout the water column, from the Mid-Ocean Dynamics Experiment (The MODE Group, 1978) to the Polygon Mid-Ocean Dynamics Experiment (PolyMode: McWilliams *et al.*, 1983; Taft *et al.*, 1986), followed by satellite altimetry (Fu *et al.*, 2010, and references therein).

Primitive-equation systems, either dynamically reduced or embodied in numerical models, support both barotropic waves and mesoscale features. Formally, a solution that fits both the observations and dynamics is determined through an assimilation process that minimizes errors to both. Thus,

given a single water-level observation, such as one obtained from a satellite altimeter, and given the primitive equations, either a barotropic wave or a mesoscale eddy is an equally acceptable solution to match both the observation and dynamics. However, if observations were of one dynamical process and yet interpreted as the other, an unsatisfactory solution would result. Thus, additional information is needed to guide the solution, originating from experience in ocean forecasting, and resulting in a rigorous methodology for specification of errors within the ocean dynamical system at hand. In the context of a three-dimensional variational (3D-Var) data assimilation, Jacobs *et al.* (2014) showed that a more accurate solution can be obtained by modifying some of the assumptions about the background error covariance. This study examines the underlying assumptions that guide a weak constraints four-dimensional variational (4D-Var) data assimilation solution toward correcting the mesoscale field, the pitfalls that occur if the assumptions are ignored, and how the assumptions lead to consistency with prior observations. In this study we consider the problem of directly assimilating sea-surface height (SSH) observations using a weak constraints 4D-Var with a free-surface ocean model, and propose a dynamically consistent approach for extracting the mesoscale circulation features that accurately match assimilated and independent observations, while avoiding the generation of gravity waves.

Successful assimilation of along-track SSH observations into ocean models has been achieved with sequential methods, e.g. the 3D-Var data assimilation and the ensemble Kalman filter (EnKF) of Evensen (1994) and its many flavours. In 3D-Var, SSH observations can be assimilated via a vertical projection of the SSH onto profiles of temperature (T) and salinity (S), i.e. synthetics (Troccoli and Haines, 1999; Segsneider *et al.*, 2001; Fox *et al.*, 2002). The difficulty with synthetics is that the correlations are built using historical observations or historical mode runs and, as such, synthetics represent average conditions rather than synoptic conditions, which may be quite different. Also, since the synthetics represent average conditions, high observation errors are used for the subsurface T and S profiles derived from the SSH observations. Relationships between the SSH and the subsurface T and S can also be introduced into the background error covariance as in Cooper and Haines (1996), or through a geostrophic balance operator as in Weaver *et al.* (2005) and Oschlies and Willebrand (1996). Again, the covariance structures are typically based on historical information and suffer the deficiency of representing average conditions. The correlation between the SSH and the subsurface T and S is explicitly taken into account in the background error covariance computed from an ensemble of model solutions. Thus, the assimilation of along-track SSH observations using an EnKF-like method does not need synthetics or the other aforementioned vertical projection methods.

Most of the above methods are subsets of the generalized 4D-Var problem that computes an optimal trajectory that best matches both the dynamical equations and observations with prescribed error covariances. There is an absence of publications dealing with direct assimilation of along-track SSH observations in free-surface ocean models using the 4D-Var method without gravity waves. A few prior 4D-Var experiments that have encountered the problem of the generation of surface gravity waves when attempting to assimilate along-track SSH observations into free-surface models include: Powell *et al.* (2009) and Matthews *et al.* (2012). Stammer *et al.* (2002) note about their analysed SSH anomalies in their Fig. 14 that '*the displayed fields were smoothed over 10 days to suppress vigorous barotropic signal that would otherwise dominate*'. Although not using 4D-Var, other studies have encountered and reported this issue: Fischer (1996), Fischer *et al.* (1997) and Schöttle (2002). The following are a few ways that the SSH observations are assimilated using 4D-Var, as found in the literature.

1. One method is the assimilation of synthetic profiles of temperature and salinity (derived from SSH through regression) in 4D-Var (Ngodock and Carrier, 2013, 2014a).

Although only the steric component of SSH can be recovered, this approach clearly avoids the gravity waves problem because innovations times Dirac impulses are always forcing the adjoint of the subsurface temperature and salinity equations, and never the free surface.

2. Another method is the assimilation of SSH maps (Powell *et al.*, 2008, 2009; Ferron, 2011; Moore *et al.*, 2011). SSH maps are produced by a two-dimensional interpolation of the along-track observations spanning a certain time period, e.g. 10 days. The maps pre-impose a covariance on the data. From the context of the 4D-Var, which attempts to take into account the observations and dynamics simultaneously, the use of gridded maps presupposes some structure on the error covariances. Usually, maps are constructed without a model background and are not synoptic. This bypasses a dynamics-based forecast that can provide a better background for the data. Gravity waves are avoided in the assimilation of maps because a rather smooth field of impulses is supplied to the adjoint model instead of sparse and localized impulses.
3. The derivation of geostrophic velocities computed as along-track gradients of the SSH observations was proposed earlier by Forbes and Brown (1996). This idea avoids the generation of gravity waves because when the SSH observations are converted to surface velocity observations, the latter may be assimilated in the top layer of the baroclinic mode. Thus, there are no Dirac impulses associated with the SSH observations forcing the adjoint of the free-surface equation.
4. Recently, Kurapov *et al.* (2011) and Yu *et al.* (2012) assimilated SSH slopes using a 4D-Var system. SSH slopes can be interpreted as geostrophic velocities since their computation is identical. The difference between the assimilation of the velocities and the slopes is that in the latter the observation operator is a function of the SSH, and as such, Dirac impulses will appear in the right-hand side of the adjoint of the free-surface equation. In this case, the adjoint solution will be contaminated by gravity waves as evidenced in Fig. 15 of Kurapov *et al.* (2011) and Fig. 7 of Yu *et al.* (2012). These gravity waves do not seem to have adversely affected their solution because (i) the SSH slopes were assimilated as daily averages, i.e. the adjoint free-surface equation was forced by a fraction of the overall impulse magnitude at every adjoint time step, and (ii) only the initial condition was corrected; some of the gravity waves energy had dissipated.
5. Finally an attempt to avoid the generation of gravity waves was proposed by Matthews *et al.* (2012); it consists of repeatedly assimilating the same SSH observation multiple times, e.g. at $t_0 - 6$ h, $t_0 - 4$ h, $t_0 - 2$ h, t_0 , $t_0 + 2$ h, $t_0 + 4$ h and $t_0 + 6$ h instead of assimilating the observation at t_0 only. The authors state that this method is adopted to prevent spurious gravity waves from being added during the assimilation. So, rather than properly considering the problem, this method seeks a solution in which long time period errors were imposed by making up information that had not been observed. It is our belief that in a properly designed assimilation system each observation should be assimilated only once, at the time that the observation is recorded to have been made, especially for observations that have a direct linear relationship with a model prognostic variable as is the case here with SSH observations and surface elevation in a free-surface model.

An approach for directly assimilating along-track SSH observations using a weak constraints 4D-Var without generating surface gravity waves is proposed in this study. The proposed approach is tested in an assimilation experiment carried out in the Gulf of Mexico, and an evaluation is made to demonstrate that gravity waves are absent in the assimilated solution and the latter fits both the assimilated and unassimilated data accurately.

The remainder of the article is organized as follows: the free-surface mode and its adjoint are briefly described in section 2, and the assimilation system in section 3. Section 4 deals with the assimilation experiments and results, and concluding remarks follow in section 5.

2. The free-surface mode and its adjoint

The equations for a linearized free-surface mode of an ocean model can be written as

$$\frac{\partial D\bar{u}}{\partial t} + gD\frac{\partial}{\partial x}\zeta = D\bar{G}_u, \tag{1}$$

$$\frac{\partial D\bar{v}}{\partial t} + gD\frac{\partial}{\partial y}\zeta = D\bar{G}_v, \tag{2}$$

$$\frac{\partial \zeta}{\partial t} + \frac{\partial}{\partial x}D\bar{u} + \frac{\partial}{\partial y}D\bar{v} = D\bar{Q}, \tag{3}$$

where ζ is the surface elevation, D is the depth, the bar over variables denotes the vertical integral, \bar{u} and \bar{v} are the barotropic velocities, $D\bar{G}_u$ and $D\bar{G}_v$ are the vertical integrals of all the tendency terms of the zonal and meridional components of the baroclinic momentum equations, respectively, with the exception of the surface elevation gradient terms and the vertical mixing. The quantities $D\bar{G}_u$ and $D\bar{G}_v$ include such terms as advection, the Coriolis effect and the external atmospheric forcing. Likewise, $D\bar{Q}$ is the vertical integral of the volume source terms (e.g. river inflow) in the continuity equation for the volume conservation in each layer. Equations (1)–(3) are written in terms of barotropic transports and an implicit time-stepping scheme can be used for the numerical solution, resulting in an elliptic equation. Not only do the terms on the right-hand side (hereafter rhs) of Eqs (1), (2) and (3) represent the baroclinic forcing on the barotropic mode, they also determine the dynamical balance between the two modes. Thus, the presence of any additional term (in the form of perturbation or forcing) on the rhs of Eqs (1), (2) and (3) that is not the vertical integral of terms in the baroclinic mode will result in the generation of surface gravity waves, because such a term will violate the dynamical balance between the two modes. In other words, one cannot add a forcing or perturbation to the barotropic mode independently of the baroclinic mode without generating surface gravity waves, especially when the perturbation is instantaneous and localized. The potential to generate surface gravity waves under these circumstances is inherent to all free-surface models, and does not depend on the time-stepping scheme used in the numerical solution of the free-surface mode. When radiative conditions are prescribed at open boundaries of a regional limited-area model, the gravity waves will propagate (fast) outside of the model domain. However, for semi-enclosed domains these waves will reflect and propagate back into the domain. If perturbations are introduced over time and at different locations there will be a superposition (a linear combination) of the waves that will significantly distort the SSH field.

The adjoint model of the free surface mode takes the form

$$-\frac{\partial \lambda_{D\bar{u}}}{\partial t} - \frac{\partial \lambda_\zeta}{\partial x} = \dots, \tag{4}$$

$$-\frac{\partial \lambda_{D\bar{v}}}{\partial t} - \frac{\partial \lambda_\zeta}{\partial y} = \dots, \tag{5}$$

$$-\frac{\partial \lambda_\zeta}{\partial t} - g\frac{\partial D\lambda_{D\bar{u}}}{\partial x} - g\frac{\partial D\lambda_{D\bar{v}}}{\partial y} = \dots, \tag{6}$$

$$\lambda_{\bar{G}_u} = D\lambda_{D\bar{u}}, \tag{7}$$

$$\lambda_{\bar{G}_v} = D\lambda_{D\bar{v}}, \tag{8}$$

$$\lambda_{\bar{Q}} = D\lambda_\zeta, \tag{9}$$

where $\lambda_{D\bar{u}}$, $\lambda_{D\bar{v}}$ and λ_ζ are the adjoint variables associated with the barotropic transports $D\bar{u}$, $D\bar{v}$ and the surface elevation ζ respectively, and $\lambda_{\bar{G}_u}$, $\lambda_{\bar{G}_v}$ and $\lambda_{\bar{Q}}$ are the adjoint variables associated with the vertically integrated baroclinic tendency terms \bar{G}_u , \bar{G}_v and \bar{Q} . The equations for the adjoint of the barotropic mode (4)–(6) are similar to those of the forward barotropic mode (1)–(3), except for some coefficients and the negative signs in the left-hand sides. Thus, the adjoint barotropic mode will exhibit a similar behaviour as the forward barotropic mode under similar localized forcing.

By definition, the adjoint computes the sensitivity of a given function of the state variables to all of the model variables when the Jacobian of the said function is placed in the rhs of the adjoint model (Cacuci *et al.*, 1980; Errico, 1997; Le Dimet *et al.*, 1997). For a function of SSH at one grid point in the domain, the adjoint solution will display the sensitivity of that function to all model dynamics, both barotropic and baroclinic, where the sensitivity to the barotropic dynamics is governed by Eqs (4)–(6) and takes the form of surface gravity waves, while sensitivity to the baroclinic dynamics is propagated from the adjoint of barotropic variables to the adjoint of the baroclinic variables via $\lambda_{\bar{G}_u}$, $\lambda_{\bar{G}_v}$ and $\lambda_{\bar{Q}}$. Although not desired, these gravity waves are part of the mechanism by which information propagates in the domain to contribute to SSH variations.

3. The assimilation procedure

The potential generation of surface gravity waves from both the free-surface mode and its adjoint becomes a compound problem when assimilating SSH observations with 4D-Var. Assume that the ocean model can be written in the generic form

$$\left. \begin{aligned} \frac{\partial X}{\partial t} &= F(X) + f, \quad 0 \leq t \leq T \\ X(t=0) &= I(x) + i(x) \end{aligned} \right\}, \tag{10}$$

where X stands for all the dependent model state variables, i.e. the two-dimensional SSH and barotropic velocities, and the three-dimensional temperature, salinity, and baroclinic velocities, F includes the model tendency and forcing terms, f is the model error with covariance C_f , $I(x)$ is the prior initial condition, and $i(x)$ is the initial condition error with covariance C_i , x and t represent the position in the three-dimensional space and time respectively. Given a vector y of M observations of the model state in the space–time domain, with the associated vector of observation errors ϵ (with covariance C_ϵ),

$$y_m = H_m X + \epsilon_m, \quad 1 \leq m \leq M, \tag{11}$$

where H_m is the observation operator associated with the m th observation, one can define a weighted cost function

$$\begin{aligned} J &= \int_0^T \int_\Omega \int_0^T \int_\Omega f(x, t) W_f(x, t, x', t') f(x', t') dx' dt' dx dt \\ &+ \int_\Omega \int_\Omega i(x) W_i(x, x') i(x') dx' dx + \epsilon^T W_\epsilon \epsilon, \end{aligned} \tag{12}$$

where Ω denotes the model domain, the weights W_f and W_i are defined as inverses of C_f and C_i in a convolution sense, and W_ϵ is the matrix inverse of C_ϵ . Boundary condition errors are omitted from Eqs (10) and (12) only for the sake of clarity. The solution of the assimilation problem, i.e. the minimization of the cost function Eq. (12) is achieved by solving the following Euler–Lagrange (EL) system:

$$\left\{ \begin{aligned} \frac{\partial X}{\partial t} &= F(X) + C_f \bullet \lambda, \quad 0 \leq t \leq T, \\ X(t=0) &= I(x) + C_i \circ \lambda(x, 0) \\ -\frac{\partial \lambda}{\partial t} &= \left[\frac{\partial F}{\partial X}(X) \right]^T \lambda + \sum_{m=1}^M \sum_{n=1}^M W_{\epsilon, mn} (y_m - H_m X), \\ &\delta(x - x_m) \delta(t - t_m), \quad 0 \leq t \leq T \\ \lambda(T) &= 0 \end{aligned} \right. \tag{13}$$

where λ is the adjoint variable defined as the weighted residual

$$\lambda(x, t) = \int_0^T \int_{\Omega} W_f(x, t, x', t') f(x', t') dx' dt', \quad (14)$$

and δ denotes the Dirac delta function, $W_{\varepsilon, mn}$ are the matrix elements of W_{ε} , the superscript T denotes the transposition, and the covariance multiplication with the adjoint variable is the convolution

$$C_f \bullet \lambda(x, t) = \int_0^T \int_{\Omega} C_f(x, t, x', t') \lambda(x', t') dx' dt', \quad (15)$$

and

$$C_i \circ \lambda(x, 0) = \int_{\Omega} C_i(x, x') \lambda(x', 0) dx', \quad (16)$$

for the model and initial condition errors respectively.

Although all types of oceanic observations can be included in Eqs (11) and (13), the discussion below is focused on SSH observations. Free-surface ocean models offer the advantage of a linear observation operator between the free-surface height from the model and SSH observations, reducing H_m to a linear interpolation from the model grid to the SSH observation locations (this usually involves only the few model grid points in the close vicinity of the observations). So, in the context of assimilating SSH observations with the 4D-Var algorithm, the rhs of the adjoint model in Eq. (13) will include a corresponding term that will appear in the rhs of the adjoint of the free-surface equation (6) and consists of Dirac delta functions (impulses) centred at the few model grid points (in space and time) used in the interpolation. As discussed above, this localized and impulsive forcing of the adjoint free-surface will yield an adjoint solution that contains surface gravity waves. It can be seen in Eq. (13) that the adjoint model is forced by the innovations (model–data misfits at the observation locations), and its solution initializes and/or forces the forward model, depending on whether a strong or weak constraints assumption is adopted. Thus gravity waves generated in the adjoint of the free-surface mode when forced by SSH innovations will be passed on to the forward solution either as an initial condition or as forcing according to Eq. (13). This in turn will generate surface gravity waves in the forward solution as discussed above, unless care is taken to ensure that the adjoint free-surface elevation is dynamically balanced with the adjoint baroclinic mode. Surface gravity waves, however, cannot be balanced with the baroclinic mode. Therefore, if SSH observations are to be assimilated with 4D-Var to estimate the mesoscale circulation, surface gravity waves have to be removed from the forward solution of the free-surface mode. We now outline how this can be achieved.

3.1. Strong constraints 4D-Var

The strong constraints 4D-Var method (Le Dimet and Talagrand, 1986; Courtier, 1997) consists of setting C_f to zero and solving the Euler–Lagrange equations (13) by iteratively correcting the initial conditions (control variables) using a gradient descent approach, the gradient of the cost function being conveniently supplied by the term $C_i \circ \lambda(x, 0)$, i.e. the adjoint solution at the initial time of the assimilation window convolved with the initial condition error covariance. In theory this term equally applies to all initial conditions assumed to be erroneous in the model. Since unbalanced changes in the initial conditions for the free surface can trigger gravity waves, a straightforward way to avoid the latter is not to include a correction to the initial condition for the free surface, i.e. to assume that the initial condition for the free surface does not have errors. Thus, initial condition errors are assumed and corrected by the assimilation only in the baroclinic mode, and the free-surface mode will dynamically adjust to those corrections

according to the inherent relationships in the model equations. This amounts to setting the background error covariance for the barotropic mode to zero. Note that the correction to the initial condition of the free-surface elevation contains both barotropic and baroclinic components. The removal of this correction term will not only have the positive effect of avoiding the generation of surface gravity waves, but also the negative effect of discarding the baroclinic contribution to the correction of the free surface at the initial time, which will cause transients such as inertial oscillations while the free surface adjusts to the baroclinic mode. The solution to the latter problem is the inclusion of a balance operator constraint (Weaver *et al.*, 2005) in the initial error covariance.

3.2. Weak constraints

In weak constraints 4D-Var, the term $C_f \bullet \lambda(x, t)$ is added to the rhs of the forward model for the correction of the model or forcing errors, in addition to the initial conditions correction term discussed above for the strong constraint. This also equally applies, in theory, to all model equations that are assumed to contain errors. Here also we note that the inclusion of a model error correction term in the rhs of the free-surface mode will trigger the unwanted gravity waves. However, the avoidance of the gravity waves is not the only reason why this term should not be included in the rhs of the free-surface mode. The latter is externally and internally forced by freshwater fluxes and the baroclinic mode respectively. We assume that the freshwater fluxes cannot account for mesoscale variability, and consider the freshwater flux errors are negligible, compared to errors associated with misplaced mesoscale eddies and fronts. Thus, for the correction of the mesoscale circulation, what are thought of as errors in the barotropic mode should actually be the vertically integrated errors of the baroclinic mode. Because the baroclinic error correction is part of the baroclinic tendency terms, its vertical integral is automatically included in the rhs of the barotropic mode so that the latter does not need a separate error correction term of its own. If one could perhaps interpret the removal of the initial condition error term in the free surface as a matter of convenience to avoid gravity waves, the same cannot be said for the model error term, which is a matter of internal dynamical consistency coming from the model formulation of the free surface.

3.3. Representer method

Allowing model error increases the dimension of the control space and the computational cost of the assimilation, and usually renders the minimization process poorly conditioned. This difficulty may be avoided if the minimization is carried out in the data space which does not depend on, and is usually smaller than, the control space. That is possible through the representer algorithm (Bennett, 1992, 2002), which expresses the solution of the EL system as the sum of a first guess and a finite linear combination of representer functions, one per datum. A representer function associated with a single SSH observation is computed by solving the adjoint model forced by a Dirac delta function centred at the observation location, then using the convolved adjoint (with initial and model error covariances) according to Eq. (13) to solve the tangent linear model instead of the nonlinear forward model as in Eq. (13). It follows that once gravity waves contaminate the representer functions they will also contaminate the entire assimilation solution. The representer algorithm cannot be applied to Eq. (13) directly mainly because of its nonlinear nature. However, following Ngodock *et al.* (2000) and Bennett (2002), the representer algorithm can be applied to a linearized form of Eq. (13), which is obtained either by linearizing Eq. (13) directly or by linearizing the forward model Eq. (10) and deriving an EL associated with the cost function based on the linearized forward model. See Ngodock and Carrier (2014b) for

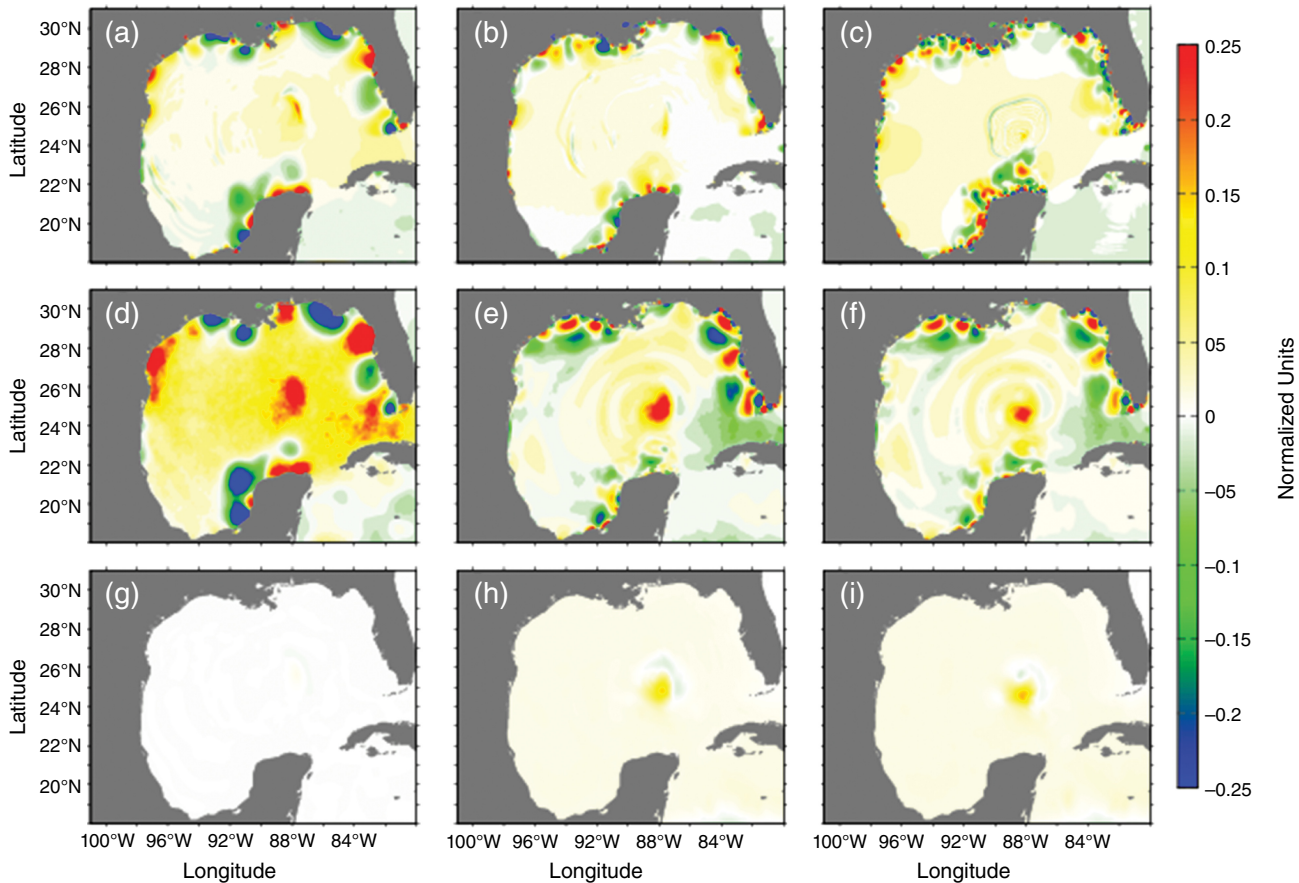


Figure 1. An example of gravity waves in the adjoint free-surface solution 96, 48 and 3 h into the adjoint integration respectively (a–c), and the corresponding free surface for the forward solutions at the corresponding adjoint times, one forced with the adjoint solution (d–f) and the other without adjoint forcing of the free surface (g–i).

more details on the linearized form of Eq. (13) and the equations for computing representer functions.

From the considerations above, we propose a system in which neither initial condition nor model errors are assigned to the free surface, and that results in the elimination of the gravity waves from the analysis as shown below.

An example of gravity waves in the adjoint and forward solutions of the free-surface elevation is shown in Figure 1 for an SSH impulse located at (24.43°N, 271.38°E) at 0000 UTC on 15 September 2012. The numerical representation of the impulse is $1/(\Delta x \Delta y \Delta T)$, where $\Delta x = \Delta y = 6$ km, $\Delta T = 3$ h. The adjoint model is integrated backward in time for 5 days to 0000 UTC 10 September 2012. The adjoint solution is shown for 96, 48 and 3 h into the integration (Figure 1(a), (b) and (c) respectively). Gravity waves can be seen emanating from the impulse location with a significant portion of the wave energy trapped along the coast of the semi-enclosed domain. The waves persist but dissipate with time; only a small portion of the waves' energy remains at day 5, the end of the adjoint integration (which is the initial time of the assimilation window). This may be the reason why strong constraints methods do not severely suffer from the gravity waves problem. Also shown in Figure 1 are the two forward free-surface elevation solutions (for the corresponding adjoint times), one with adjoint forcing (d)–(f) that is affected by gravity waves, and the other without adjoint forcing (g)–(i) and not affected by gravity waves. Note that according to the representer method, the final SSH increments from the data assimilation process are a linear combination of forward solutions such as those shown in Figure 1.

4. Experiments

In the experiments described below, the assimilation system is the representer-based Navy Coastal Ocean Model NCOM-4D-Var system that was described in Ngodock and Carrier (2014a) and

has been used to assimilate real observations in Monterey Bay (Ngodock and Carrier, 2014b) and in the Gulf of Mexico (Carrier *et al.*, 2014). The model domain for this experiment extends from 79 to 98°W and 18–31°N using a spherical coordinate projection at a horizontal resolution of 6 km. The model has 50 layers in the vertical, with 25 free-sigma levels extending to a depth of 116 m and constant z -levels extending down to a maximum of 5500 m with the depth of the first subsurface layer at 0.5 m. Initial and lateral boundary conditions are provided by the global NCOM at 1/8° resolution (every 3 h) and surface atmospheric forcing, such as wind stress, atmospheric pressure and surface heat flux is provided by the 0.5° Navy Operational Global Atmospheric Prediction System (NOGAPS) model every 3 h (Rosmond *et al.*, 2002); river forcing is provided at all river inflow locations in the Gulf of Mexico domain.

The assimilation window covers the 20-day interval from 10 to 30 September 2012. The observations being assimilated consist of sea-level anomalies (SLA) from satellite altimetry, GOES-East sea-surface temperatures (SST), ARGO profiling floats (Roemmich *et al.*, 2001), Expendable Bathythermographs (XBT) and drifting buoys. SLA observations are converted to SSH by adding a mean SSH field. Observations are processed in bins of 6 h. The assimilation is carried out in four sequential cycles of 5 days, where the analysis at the end of one cycle becomes the initial condition for the forecast/background for the following cycle, and the background for the first cycle is the model solution integrated from the initial condition on 10 September 2012.

The representer method is used for the minimization of the cost function, and the details of the assimilation process are described in Ngodock and Carrier (2014a). Prescribed errors for the initial conditions are 1 °C, 0.1 PSU (practical salinity unit), and 0.5 m s⁻¹ for temperature, salinity and the two components of velocity respectively, and the prescribed model errors are 0.05 °C, 0.04 PSU, and 0.1 m s⁻¹, which correspond to 10% of the magnitude of the forcing fields. For the experiment with adjoint

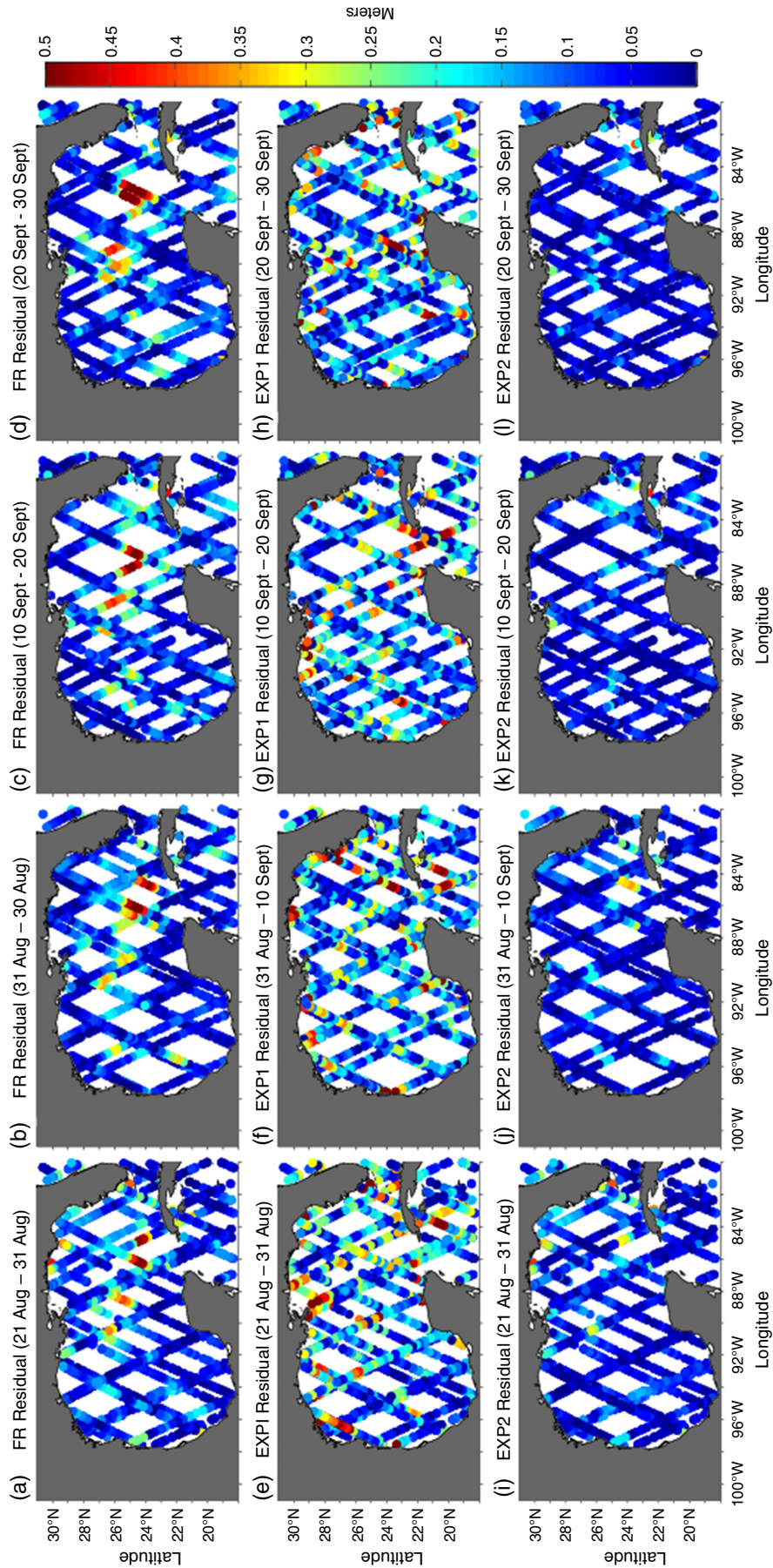


Figure 2. A comparison of absolute innovations (a–d) and absolute analysis residuals from EXP1 (e–h) and EXP2 (i–l) for each assimilation cycle respectively.

forcing included in the forward free-surface equation, an initial condition of 0.2 m is prescribed, as well as a model error of 0.15 m representing 10% of the magnitude of the vertically integrated volume flux source. The model error units have been converted from flux units to those of the ocean state through multiplying constants from the discretized model as detailed in Ngodock and Carrier (2013, 2014b).

Observation errors are set to 0.3 °C, 0.1 PSU and 0.05 m for temperature, salinity and SSH respectively, and are held constant. Also, the observations error covariance matrix is diagonal. Both the initial condition and the model errors have a spatial decorrelation scale of 30 km, and the time decorrelation scale of 3 days is assigned to the model error. Also, observations are subsampled according to the horizontal correlation scale (such that only one observation per type within the correlation length is retained for assimilation) and stored every six hours as they become available.

Two assimilation experiments are carried out: the assimilation of all observations with adjoint forcing included in the free surface (hereafter referred to as EXP1), and the assimilation of all observations without adjoint forcing included in the free surface (hereafter referred to as EXP2). The results of these two experiments are examined in various ways below.

The comparison between EXP1 and EXP2 begins with the examination of all along-track SSH innovations and the corresponding analysis residuals for each cycle. It should be noted that after the first cycle, EXP1 and EXP2 produce different first guesses for subsequent cycles (resulting from the different analyses), and therefore different innovations. However, the innovation statistics are similar from both experiments (not shown), and thus only the innovations from EXP1 are retained in this along-track comparison. It can be seen in Figure 2 that in the first cycle, EXP1 struggles to fit the observations; more than half of the locations have an analysis residual of more than 10 cm (two observations error standard deviations), with several locations exceeding 25 cm. Although the fit to observations from EXP1 improves in the subsequent cycles, analysis residuals of more than 10 cm still appear at several locations, and some exceeding 20 cm, e.g. in the fourth cycle. On the other hand, analysis residuals from EXP2 are generally well below the SSH observation error of 5 cm, with a few locations where they exceed 10 cm.

In order to assess the fit to the observations over time in the whole assimilation window, we define the following ‘fit to the observations’ metric:

$$J_{\text{FIT}} = \frac{1}{M} \sum_{m=1}^M \frac{|y_m - H_m X^a|}{\sigma_m}. \quad (17)$$

In Eq. (17) y_m is the m th observation, M is the total number of observations, H_m is the observation operator, X^a is the assimilated solution or analysis, and σ_m is the observation error or standard deviation (std). The rhs of Eq. (17) can be computed as a time series, and also evaluated for the free-run solution and the first guess. Because the assimilation is expected to fit the observations to within the observation standard deviation at the observation locations, the metric J_{FIT} in Eq. (17) is expected to be less or equal to 1 for the analysis. One only hopes that the same is true for the subsequent forecasts as a result of fitting the observations in previous cycles. The values of J_{FIT} represent the number of observation error std by which any solution departs from the observations. They are computed with along-track SSH observations as shown in Figure 3 (as a time series) for the free-run solution and the analyses from EXP1 and EXP2. It can be seen that the free run does not agree with the observations at all. With the exception of a few time levels, J_{FIT} values for the free run are generally greater than 1.5, occasionally exceeding 2.5, and have a time-averaged value of 2.06. For the assimilated solution of EXP1, J_{FIT} values are generally lower than 2 (an improvement from the free run), occasionally lower than 1, with a time average

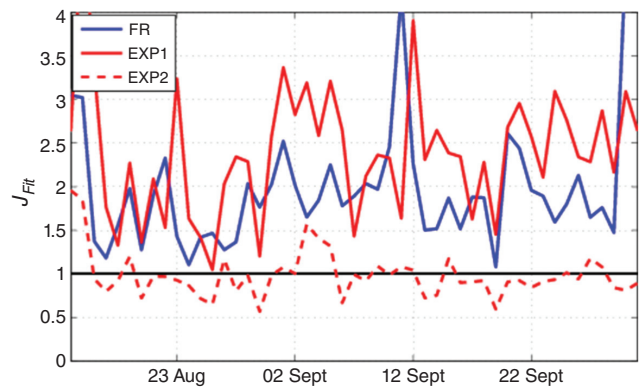


Figure 3. Time series of the J_{FIT} metric for the free run (blue), the analysis from EXP1 (red, solid line) and from EXP2 (red, dashed line).

of 1.47. EXP2 produces an assimilated solution for which J_{FIT} values are generally below 1, only exceeding 1 to reach 1.25 on two occasions, around 11 and 27 September, with a time average of 0.6. It is clear from these J_{FIT} values that contrary to EXP2, EXP1 fails to accurately fit the assimilated SSH observations, and this is attributed to the inclusion of adjoint forcing in EXP1, since it is the only difference between the two assimilation experiments.

We now compare these two analyses over the entire domain in order to examine how they represent the SSH away from the observation locations. In the absence of independent SSH observations, we resort to Archiving, Validation and Interpretation of Satellite Oceanographic data (AVISO) maps. The latter are by no means a better product, since they are obtained from two-dimensional interpolation in space and over time. However, they do offer a reasonable quick-look of the SSH field away from the locations of the assimilated observations, allowing the assimilated solutions to be evaluated beyond the observation locations. A comparison of the SSH field from AVISO, EXP1 and EXP2 at the end of each assimilation cycle is shown in Figure 4. It can be seen that most of the large-scale features in the AVISO maps are represented in the EXP2 analysis at all four time levels. EXP1 displays similar features, but with significant small-scales distortions along the coast as well as in the domain interior. Also, EXP1 displays a few large-scale features that are not seen in the AVISO or EXP2 maps, e.g. the elongated cyclonic circulation in the northwestern Gulf at the end of the first cycle, a similar feature in the northern Gulf south of the Mississippi river delta at the end of the second cycle, and the low SSH features in the Bay of Campeche at the end of the third cycle.

Similar to the evaluation of the assimilation experiments at the observation locations in Figure 3, the J_{FIT} values are also computed with the AVISO fields taking the place of the observations. It is shown in Figure 5 that the SSH analysis from EXP2 is very close to the AVISO SSH, the spatially averaged discrepancy with the latter ranging from 1 to 1.3 observations error std, with the time-averaged discrepancy of 1.21. On the other hand, the analysis SSH from EXP1 has a discrepancy with the AVISO SSH that is generally greater than 1.5, occasionally exceeding 2, with a time-averaged discrepancy of 1.87. These values are higher than their counterparts for the metric evaluated at the observation locations, indicating that in comparison to AVISO SSH maps the assimilated solution tends to deteriorate away from the locations of assimilated observations, more so with the analysis from EXP1. Thus the distortions seen above in the SSH analysis from EXP1 translate into a significant departure from the AVISO SSH, if the latter is to be trusted.

4.1. Surface drifter trajectories

Both EXP1 and EXP2 are further evaluated against truly independent observations in the form of drifter trajectories. The latter were obtained from the Grand Lagrangian Deployment (GLAD) of drifters in the Gulf of Mexico in July 2012, as

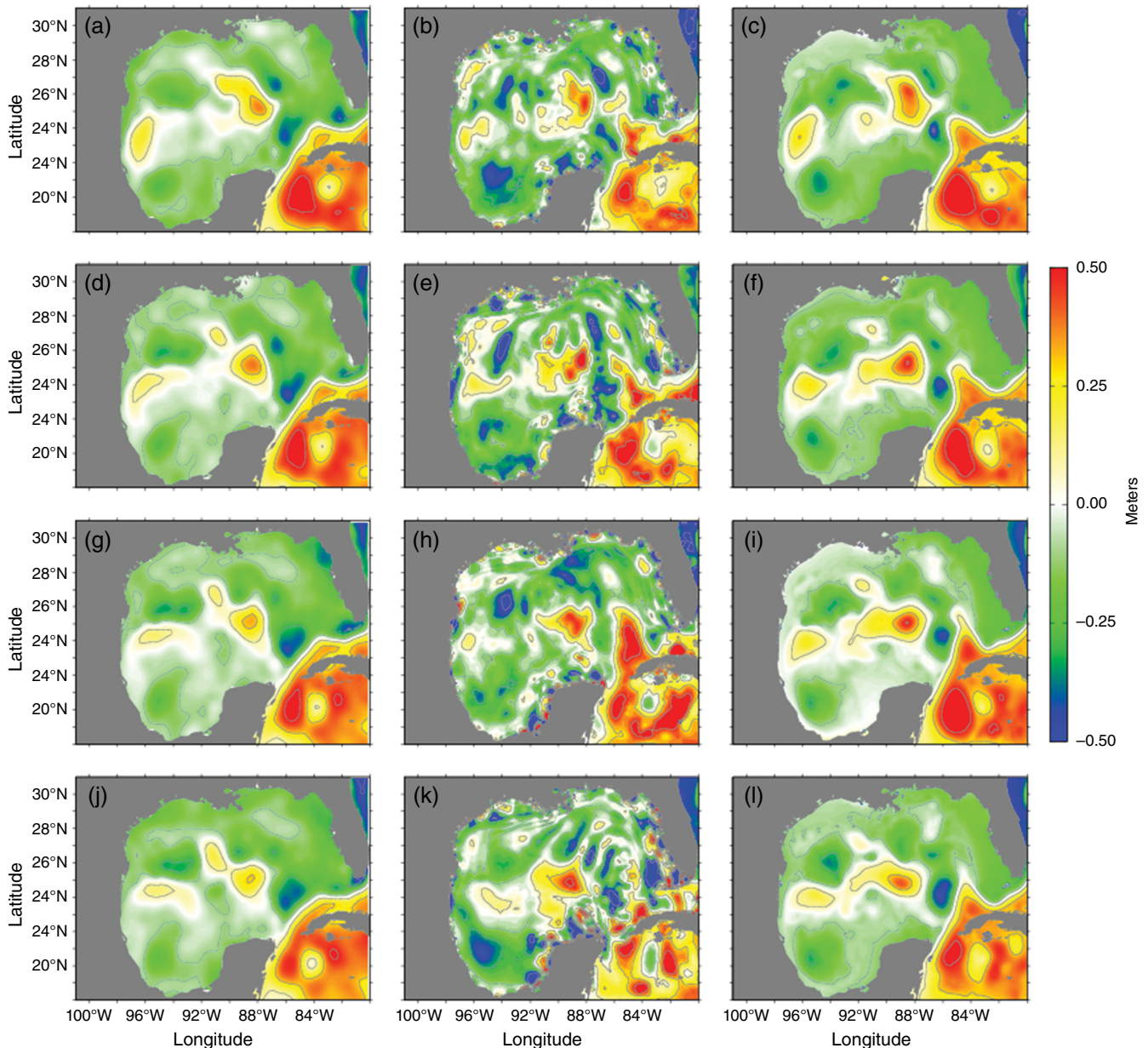


Figure 4. A comparison of the SSH fields from AVISO maps (a,d,g,j) and the analysis from EXP1 (b,e,h,k) and EXP2 (c,f,i,l) at the end of each assimilation cycle respectively.

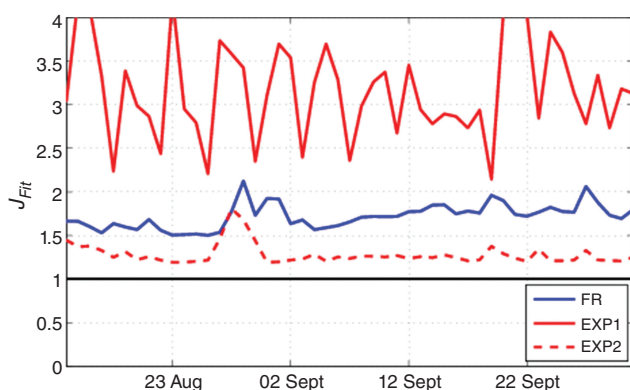


Figure 5. Same as Figure 3, except for the J_{FIT} values being computed with AVISO maps over the whole domain, instead of the observations at their locations.

part of the Consortium for Advanced Research on Transport of Hydrocarbon in the Environment (CARTHE). Surface velocities from the drifters are not assimilated in either EXP1 or EXP2, but the forecasted surface velocities from both experiments are used to compute trajectories that are compared to the observed drifter trajectories during the month of September. There is a total of 150 GLAD drifters in the Gulf of Mexico at any given time in

the month of September. A small number of drifters (10%) is randomly selected for visual comparison with 3-day forecasted trajectories, for the sake of clarity in Figure 6; more drifter positions would result in intersecting trajectories that would be difficult to distinguish from one another. Results are shown for four 3-day time windows, namely 14–17, 18–21, 22–25 and 26–29 September, in a sub-region of the Gulf of Mexico. It can be seen that of all 60 drifter positions combined from the four panels of Figure 6, 32 (or 53%) of the forecasted trajectories from EXP2 (purple lines) are closer to the observed trajectories (green lines) than the forecasted trajectories from EXP1 (red lines), compared to 13 (or 22%) of forecasted trajectories from EXP1, and 15 (or 25%) of trajectories cannot be unequivocally decided.

The evaluation of forecasted trajectories against the observed ones is expanded to all 150 drifters using the 's' index (hereafter referred to as s-index) defined by Liu and Weisberg (2011). For a single drifter, the index is obtained as the cumulative separation distance with the simulated trajectory, normalized by the cumulative distance travelled by the drifter. Comparative results of this s-index are summarized in Table 1 for separate forecast lengths of 1, 2, 3 and 4 days from 14 to 30 September, and averaged over all the 150 drifters. For all forecast lengths, EXP2 has lower s-index values than EXP1. This implies that on average the forecasted trajectories from EXP2 are always closer to the observed

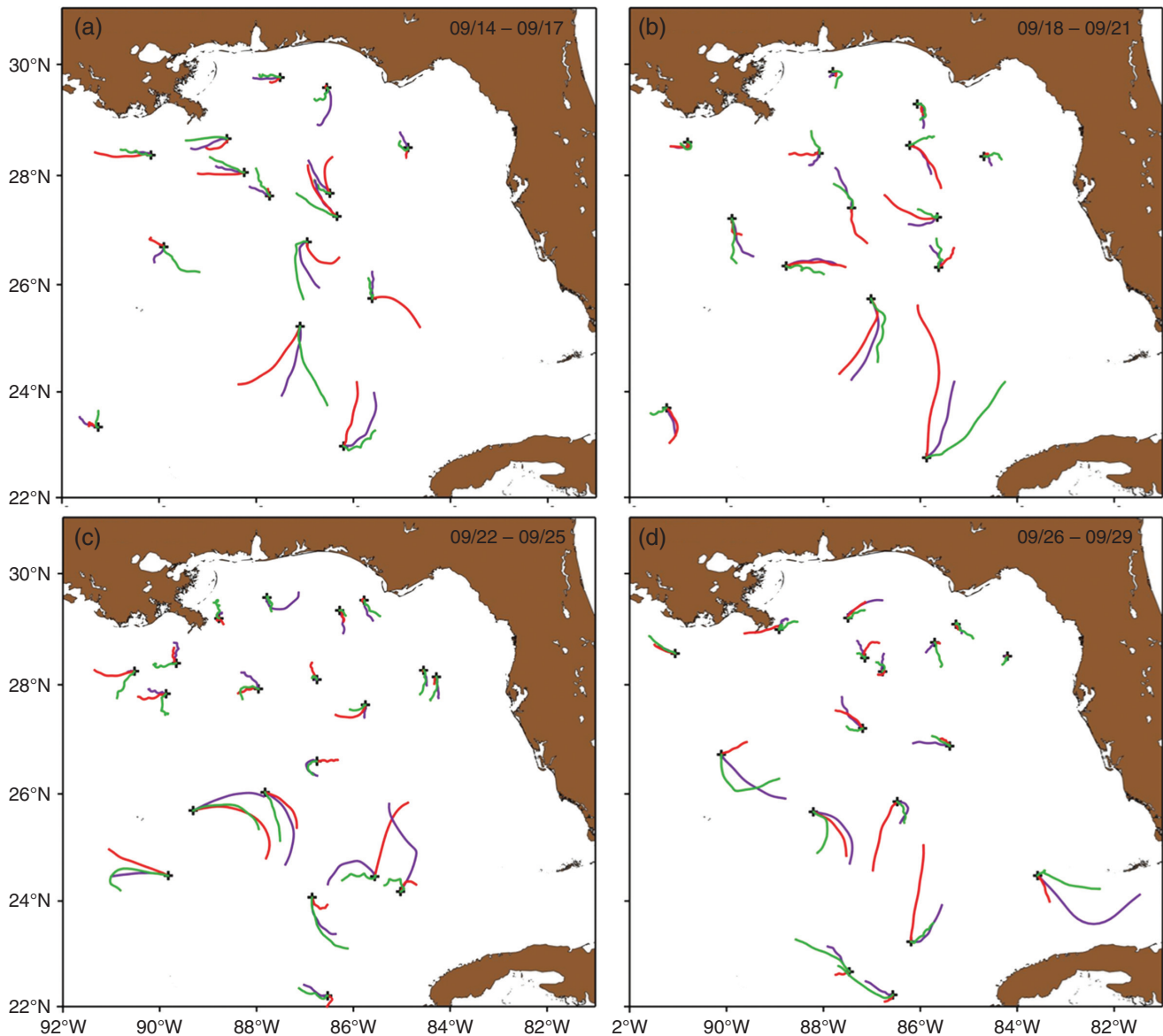


Figure 6. A comparison of observed drifter trajectories (green) with those computed from forecasted solutions from EXP1 (red) and EXP2 (purple) for the 3-day time windows of (a) 14–17, (b) 18–21, (c) 22–25, and (d) 26–29 September 2012.

Table 1. Averaged *s*-index values per forecast length from EXP1 and EXP2.

	1-day	2-day	3-day	4-day
EXP1	0.9764	0.9966	0.9719	0.9419
EXP2	0.8458	0.8616	0.846	0.8251

ones than those from EXP1, regardless of the forecast length. This comparison shows that when SSH observations are assimilated as in EXP1, the forecasted surface Lagrangian trajectories (derived from the forecasted surface velocity) also do not match the independent observations of Lagrangian trajectories as well as those from EXP2.

5. Discussion

Gravity waves are a natural response of the ocean to an impulsive forcing. This is problematic only for free-surface ocean models where the surface elevation is a prognostic variable, whereas gravity waves are inherently filtered out by models using the rigid-lid approximation. The ocean model adjoint will create gravity waves when forced by SSH impulses. The adjoint solution is then convolved with the background error covariance to produce the correction to the initial condition and forcing for the forward model (or the TLM, in the case of the representer method).

There are a few ways to mitigate gravity waves in the adjoint solution: first, it is recognized that the main errors in the ocean have time-scales similar to those of the ocean features themselves, which are long. Thus, long space and time decorrelation scales in the error covariances will filter out gravity waves. However, gravity waves may still appear in the forward solution through any initial and/or forcing correction to the barotropic equations of motion in the model. Second, balance operators (Weaver *et al.*, 2005) enforcing geostrophy can be implanted in the covariance operator to reduce the gravity wave amplitude. However, there is a detriment to this approach since it can preclude application of 4D-Var to shallow water areas where the time-scales may be relatively short or where geostrophy may not be the dominant balance. Third, the introduction of a divergence damping term (Talagrand, 1972) in the adjoint equations can also suppress the gravity waves. However, even if one were to successfully filter out the gravity waves from the adjoint solution by using long space–time correlation scales, balance constraints, or the introduction of a divergence damping term, the mere presence of an initial condition or a forcing term from the adjoint in the free-surface equation would still generate gravity waves in the forward model or TLM integration.

In this article, we propose that no adjoint initialization or forcing correction be applied to the forward model or the TLM of the barotropic equations, i.e. the barotropic mode dynamically adjusts to the variations of the baroclinic mode as the forward

model formulation dictates. The equation for the free-surface elevation in the barotropic mode expresses the conservation of mass, which in the numerical model results in the vertical velocity being related to the horizontal divergence. The time rate of change of the SSH in the model is the horizontal divergence of the vertically integrated velocity. There is no error in the equation for the conservation of mass or the relation between the SSH rate of change and the horizontal divergence of the barotropic velocity, except for errors in surface freshwater fluxes, which may be negligible in the context of correcting errors associated with misplaced mesoscale circulation eddies and fronts. The equations governing the time evolution of the barotropic velocity are derived from the vertical integral of the baroclinic momentum equations. There is no error in these equations either. The primary errors lie in the baroclinic equations of motion that are under the influence of the turbulence parametrization, the surface flux estimates, lateral friction and the bottom stress formulation. Error covariances should be applied based on expectations of where the error sources exist. Experience has shown that errors in synoptic forecasts are primarily due to errors in the evolution of the ocean baroclinic flow within mesoscale eddies rather than due to errors in the misplacement of surface barotropic gravity waves. The equation relating barotropic forcing to the vertical integral of baroclinic forcing is an example of a conservation statement in the model to which there is no error. Thus, care should be taken in ascribing errors to the correct sources and preventing spurious results such as corrections due to surface gravity waves. It is therefore assumed here that there are no model errors associated with the barotropic mode equations. Because the free-surface equations are derived from the conservation of mass as the continuity equation, this approach is in accordance with the work of Jacobs and Ngodock (2003), where it was stated that the conservative equations should not be treated as weak constraints.

6. Conclusion

Direct assimilating of along-track SSH observations into a free-surface ocean model with a 4D-Var algorithm requires that the adjoint of the free-surface mode be solved with a linear combination of Dirac delta functions in the rhs. This adjoint solution contains surface gravity waves. Also, according to the representer method for solving a weak constraints 4D-Var problem, the adjoint solution is passed on to the TLM, including the free surface, resulting in surface gravity waves that significantly distort the SSH field in the analysis. It was argued that it is redundant and inconsistent to assign independent model errors to the free surface, because the latter is the vertical integral of the baroclinic mode, and the model errors assigned to the baroclinic mode are included in the vertical integral on the rhs of the free-surface mode. A method for avoiding the generation of the surface gravity waves in the analysis was proposed in this study; it consists of the removing the adjoint of the free surface from the initial condition and rhs of the free-surface mode in the TLM. The information from the SSH observations still propagates through all the other model dynamics and variables in the baroclinic mode, resulting in the correction of the surface elevation. Two assimilation experiments were carried out in the Gulf of Mexico using the NCOM-4D-Var system: one with adjoint forcing included on the rhs of the TLM free surface, and the other without. Both analyses were evaluated against the assimilated observations and against SSH maps from AVISO, showing in both comparisons that the analysis that did not include adjoint forcing in the free surface was more accurate. The other analysis did not only suffer from the contamination of surface gravity waves, it also had SSH features that were significantly inconsistent with the AVISO maps. Another evaluation of both experiments was made using independent observations from surface drifter trajectories. It was found that the method proposed in this study yielded forecasted trajectories that were closer to the observed

ones than the other method. This study shows that when a weak constraints 4D-Var approach is considered for the assimilation of observations including along-track SSH with a free-surface model for the estimation of the mesoscale circulation, model errors should be assigned to the baroclinic mode and not to the free surface. As the vertical integral of the baroclinic tendencies forces the barotropic mode, the vertical integral of errors assigned to the baroclinic mode is inherently included in the barotropic forcing.

Acknowledgements

This work was sponsored by the Office of Naval Research, Program Element 0601153N, as part of 'A multiscale Approach for Assessing Predictability of ASW environment' and the 'NCOM-4DVAR' projects. This article is NRL paper contribution number NRL/JA/7320-14-2148. The authors would like to thank the anonymous reviewers; their comments helped in improving the quality of this article.

References

- Bennett AF. 1992. *Inverse Methods in Physical Oceanography*. Cambridge University Press: New York, NY.
- Bennett AF. 2002. *Inverse Modeling of the Ocean and Atmosphere*. Cambridge University Press: New York, NY.
- Cacuci DG, Weber CF, Oblow EM, Marable JH. 1980. Sensitivity theory for general systems of nonlinear equations. *Nucl. Sci. Eng.* **75**: 88–110.
- Carrier MJ, Ngodock HE, Smith SC, Jacobs GA, Muscarella PA, Ozgokmen T, Haus B, Lipphardt B. 2014. Impact of assimilating ocean velocity observations inferred from Lagrangian drifter data using the NCOM-4DVAR. *Mon. Weather Rev.* **142**: 1509–1524.
- Cooper M, Haines K. 1996. Altimetric assimilation with water property conservation. *J. Geophys. Res.* **101**: 1059–1077, doi: 10.1029/95JC02902.
- Courtier P. 1997. Dual formulation of four-dimensional variational assimilation. *Q. J. R. Meteorol. Soc.* **123**: 2449–2461.
- Enfield DB, Allen JS. 1983. The generation and propagation of sea-level variability along the Pacific coast of Mexico. *J. Phys. Oceanogr.* **13**: 1012–1033, doi: 10.1175/1520-0485(1983)0132.0.CO;2.
- Errico RM. 1997. What is an adjoint model? *Bull. Am. Meteorol. Soc.* **78**: 2577–2591.
- Evensen G. 1994. Sequential data assimilation with nonlinear quasi-geostrophic model using Monte Carlo methods to forecast error statistics. *J. Geophys. Res.* **99**: 10143–10162, doi: 10.1029/94JC00572.
- Ferron B. 2011. A 4D-variational approach applied to an eddy-permitting North Atlantic configuration: Synthetic and real data assimilation of altimeter observations. *Ocean Model.* **39**: 370–385.
- Fischer M. 1996. 'Der Einfluß von Datenassimilation auf ENSO Simulationen und Vorhersagen.' PhD thesis. Universität Hamburg: Germany.
- Fischer M, Latif M, Flügel M, Ji M. 1997. The impact of data assimilation on ENSO simulations and predictions. *Mon. Weather Rev.* **125**: 819–830.
- Forbes C, Brown O. 1996. Assimilation of sea surface height data into an isopycnic ocean model. *J. Phys. Oceanogr.* **26**: 1189–1213.
- Fox DN, Teague WJ, Barron CN, Carnes MR, Lee CM. 2002. The modular ocean data assimilation system (MODAS). *J. Atmos. Oceanic Technol.* **19**: 240–252.
- Fu LL, Chelton DB, LeTraon P-Y, Morrow R. 2010. Eddy dynamics from satellite altimetry. *Oceanography* **23**: 14–25, doi: 10.5670/oceanog.2010.02.
- Jacobs GA, Ngodock HE. 2003. The maintenance of conservative physical laws within data assimilation systems. *Mon. Weather Rev.* **131**: 2595–2607.
- Jacobs GA, Hurlburt HE, Kindle JC, Metzger EJ, Mitchell JL, Teague WJ, Wallcraft AJ. 1994. Decade-scale trans-Pacific propagation and warming effects of an El Niño anomaly. *Nature* **370**: 360–363, doi: 10.1038/370360a0.
- Jacobs GA, Bartels BP, Bogucki DJ, Beron-Vera FJ, Chen SS, Coelho EF, Curcic M, Griffa A, Gough M, Haus BK, Haza AC, Helber RW, Hogan PJ, Huntley HS, Iskandarani M, Judt F, Kirwan AD, Laxague N, Valle-Levinson A, Lipphardt BL, Mariano AJ, Ngodock HE, Novelli G, Orlascoaga MJ, Ozgokmen TM, Poje AC, Reniers AJHM, Rowley CD, Ryan EH, Smith SR, Spence PL, Thoppil PG, Wei MZ. 2014. Data assimilation considerations for improved ocean predictability during the Gulf of Mexico Grand Lagrangian Deployment (GLAD). *Ocean Model.* **83**: 98–117, doi: 10.1016/j.ocemod.2014.09.003.
- Johnson ES, McPhaden MJ. 1993. Structure of interseasonal Kelvin waves in the tropical Pacific Ocean. *J. Phys. Oceanogr.* **23**: 608–625.
- Knox RA, Halpern D. 1982. Long range Kelvin wave propagation of transport variations in Pacific Ocean equatorial currents. *J. Mar. Res.* **40**(Suppl.): 329–339.
- Kurapov AL, Foley D, Strub PT, Egbert GD, Allen JS. 2011. Variational assimilation of satellite observations in a coastal ocean model off Oregon. *J. Geophys. Res.* **116**: C05006, doi: 10.1029/2010JC006909.

- LeBlonde PH, Mysak LA. 1978. *Waves in the Ocean*. Elsevier: New York, NY.
- Le Dimet F-X, Talagrand O. 1986. Variational algorithms for analysis and assimilation of meteorological observations: Theoretical aspects. *Tellus* **38A**: 97–110.
- Le Dimet F-X, Ngodock HE, Luong B, Verron J. 1997. Sensitivity analysis in variational data assimilation. *J. Meteorol. Soc. Jpn.* **75**: 245–255.
- Liu Y, Weisberg RH. 2011. Evaluation of trajectory modeling in different dynamic regions using normalized cumulative Lagrangian separation. *J. Geophys. Res.* **116**: C09013, doi: 10.1029/2010JC006837.
- Luther DS. 1980. 'Observations of long period waves in the tropical oceans and atmosphere.' PhD thesis. Massachusetts Institute of Technology – Woods Hole Oceanographic Institution: Woods Hole, MA.
- McWilliams JC, Brown ED, Bryden HL, Ebbesmeyer CC, Elliott BA, Heinmiller RH, Hua BL, Leaman KD, Lindstrom EJ, Luyten JR, McDowell SE, Owens WB, Perkins H, Price JF, Regier L, Riser SC, Rossby HT, Sanford TB, Shen CY, Taft BA, van Leer JC. 1983. The local dynamics of eddies in the western North Atlantic. In *Eddies in Marine Science*, Robinson AR. (ed.): 92–113. Springer-Verlag: Berlin, Heidelberg, Germany.
- Matthews D, Powell BS, Janeković I. 2012. Analysis of four-dimensional variational state estimation of the Hawaiian waters. *J. Geophys. Res.* **117**: C03013, doi: 10.1029/2011JC007575.
- Monserrat S, Vilibić I, Rabinovich AB. 2006. Meteotsunamis: Atmospherically induced destructive ocean waves in the tsunami frequency band. *Nat. Hazards Earth Syst. Sci.* **6**: 1035–1051. www.nat-hazards-earth-syst-sci.net/6/1035/2006/ (accessed 12 August 2014).
- Moore DW. 1968. 'Planetary-gravity waves in an equatorial ocean.' PhD thesis. Harvard University: Cambridge, MA.
- Moore DW, McCreary JP. 1990. Excitation of intermediate-frequency equatorial waves at a western ocean boundary: With application to observations from the Indian Ocean. *J. Geophys. Res.* **95**: 5219–5231, doi: 10.1029/JC095iC04p05219.
- Moore AM, Arango HG, Broquet G, Edwards C, Veneziani M, Powell B, Foley D, Doyle JD, Costa D, Robinson P. 2011. The Regional Ocean Modeling System (ROMS) 4-dimensional variational data assimilation systems: Part II – Performance and application to the California Current System. *Prog. Oceanogr.* **91**: 50–73.
- Ngodock HE, Carrier MJ. 2013. A weak constraint 4D-Var assimilation system for the Navy coastal ocean model using the representer method. In *Data Assimilation for Atmospheric, Oceanic and Hydrologic applications*, Park SK, Xu L. (eds.), Vol. 2. Springer-Verlag: Berlin, Heidelberg, Germany, doi: 10.1007/978-3-642-35088-7_15.
- Ngodock HE, Carrier MJ. 2014a. A 4D-Var system for the Navy coastal ocean model. Part I: System description and assimilation of synthetic observations in Monterey Bay. *Mon. Weather Rev.* **142**: 2085–2107, doi: 10.1175/MWR-D-13-00221.1.
- Ngodock HE, Carrier MJ. 2014b. A 4D-Var assimilation system for the Navy coastal ocean model. Part II: Strong and weak constraints assimilation experiments with real observations in Monterey Bay. *Mon. Weather Rev.* **142**: 2108–2117, doi: 10.1175/MWR-D-13-00220.1.
- Ngodock HE, Chua BS, Bennett AF. 2000. Generalized inversion of a reduced gravity primitive equation ocean model and tropical atmosphere ocean data. *Mon. Weather Rev.* **128**: 1757–1777.
- Nosov MA. 2014. Tsunami waves of seismic origin: The modern state of knowledge. *Izv. Atmos. Oceanic Phys.* **50**: 474–484, doi: 10.1134/S0001433814030098.
- Oschlies A, Willebrand J. 1996. Assimilation of Geosat altimeter data into an eddy-resolving primitive equation model of the North Atlantic Ocean. *J. Geophys. Res.* **101**: 14175–14190, doi: 10.1029/95JC03801.
- Perigaud C, Delecluse P. 1992. Annual sea level variations in the southern tropical Indian Ocean from Geosat and shallow-water simulations. *J. Geophys. Res.* **97**: 20169–20178, doi: 10.1029/92JC01961.
- Powell BS, Arango HG, Moore AM, Di Lorenzo E, Milliff RF, Foley D. 2008. 4D-Var data assimilation in the Intra-Americas Sea with the Regional Ocean Modeling System (ROMS). *Ocean Model.* **25**: 130–145.
- Powell BS, Moore AM, Arango HG, Di Lorenzo E, Milliff RF, Leben RR. 2009. Near real-time ocean circulation assimilation and prediction in the Intra-Americas Sea with ROMS. *Dyn. Atmos. Oceans* **48**: 46–68.
- Roemmich D, Boebel O, Desaubies Y, Freeland H, Kim K, King B, LeTraon P-Y, Molinari R, Owens WB, Riser S, Send U, Takeuchi K, Wijffels S. 2001. ARGO: The global array of profiling floats. In *Observing the Oceans in the 21st Century*, Koblinsky CJ, Smith NR. (eds.): 248–257. Bureau of Meteorology: Melbourne, Australia.
- Rosmond TE, Teixeira J, Peng M, Hogan TF, Pauley R. 2002. Navy operational global prediction system (NOGAPS): Forcing for ocean models. *Oceanography* **15**: 99–106.
- Schöttle S. 2002. 'The impact of sea surface height data assimilation on El Niño analyses and forecasts.' PhD thesis. Max-Planck-Institut für Meteorologie: Hamburg, Germany.
- Segsneider J, Anderson DLT, Vialard J, Balmaseda M, Stockdale TN, Troccoli A, Haines K. 2001. Initialization of seasonal forecasts assimilating sea level and temperature observations. *J. Clim.* **14**: 4292–4307.
- Spillane MC, Enfield DB, Allen JS. 1987. Intraseasonal oscillations in sea level along the west coast of the Americas. *J. Phys. Oceanogr.* **27**: 217–235.
- Stammer D, Wunsch C, Giering R, Eckert C, Heimbach P, Marotzke J, Adcroft A, Hill CN, Marshall J. 2002. Global ocean circulation during 1992–1997, estimated from ocean observations and a general circulation model. *J. Geophys. Res.* **107**: 3118, doi: 10.1029/2001JC000888.
- Taft BA, Lindstrom EJ, Ebbesmeyer CC, Shen CY, McWilliams JC. 1986. Water mass structure during the POLYMODE local dynamics experiment. *J. Phys. Oceanogr.* **16**: 403–426.
- Talagrand O. 1972. On the damping of high-frequency motions in four-dimensional assimilation of meteorological data. *J. Atmos. Sci.* **29**: 1571–1574.
- The MODE Group. 1978. The mid-ocean dynamics experiment. *Deep Sea Res.* **25**: 859–910.
- Troccoli A, Haines K. 1999. Use of the temperature–salinity relation in a data assimilation context. *J. Atmos. Oceanic Technol.* **16**: 2011–2025.
- Weaver AT, Deltel C, Machu E, Ricci S, Daget N. 2005. A multivariate balance operator for variational ocean data assimilation. *Q. J. R. Meteorol. Soc.* **131**: 3605–3625.
- Yu P, Kurapov AL, Egbert GD, Allen JS, Kosro PM. 2012. Variational assimilation of HF radar surface currents in a coastal ocean model off Oregon. *Ocean Model.* **49–50**: 86–104, doi: 10.1016/j.ocemod.2012.03.001.